Effect of Pulsed Magnetic Treatment on the Corrosion of Titanium

Anatolii Babutskyi[a], Andreas Chrysanthou[a], Maria Smelina[a], Gennadii Stepanov[b], Maciej Ziętara[c]

[a] School of Engineering and Technology, University of Hertfordshire, UK

[b] Institute for Problems of Strength of NASU, Ukraine

[c] AGH University of Science and Technology, Poland

Results of corrosion tests of titanium in the initial state and after treatment using pulsed magnetic field are presented. It is shown that samples after treatment have better corrosion resistance due to the formation of denser and finer corrosion products with better adhesion to the substrate. Samples after treatment have more homogeneous microstructure due to a substantial increase of dislocations which are uniformly distributed. Mechanisms of dislocation multiplication and a model explaining the effect of the treatment on the corrosion are discussed.

Key words: titanium, pulsed magnetic field, pulsed electric current, corrosion, dislocation multiplication, residual stresses, microhardness scattering

Introduction

Titanium and its alloys are used in a variety of applications in dentistry including orthodontic and dental hardware like bonding systems and brackets, attachments, ligatures, implants, arch wire, bulk dental wire, etc. Protection against corrosion is of paramount importance; while titanium used in dental applications can exhibit good corrosion resistance to saline solutions and body fluids, it can suffer potential attack by fluorides that are contained in toothpastes and mouthwashes[1-4].

The wet (electrochemical) corrosion mechanism involves generation of short-circuited micro-galvanic anode-cathode couples leading to corrosion and material loss. Such anode-cathode

couples can be generated because of variations in the metal structure, surface roughness, grain size and composition, surface defects and in particular non-uniform mechanical stresses and residual stresses[5, 6].

Earlier research has shown that the use of pulsed electric current (PEC) and pulsed magnetic field (PMF) treatment can lead to relaxation of mechanical stresses in metals[7-11]. Some consensus has been reached that the reason for the relaxation of stresses is the increased mobility of dislocations caused by the treatments. Such research findings can serve as the basis for the development of new technology for the corrosion protection of metals. Literature data about this type of application are quite limited. The results of earlier investigations by the present authors have demonstrated increases in the corrosion resistance of high-strength low-alloy steel (HSLA)[12] as well as steel used as concrete reinforcement[13]. At the same time, the enhanced effect of the treatment on the corrosion resistance cannot be attributed only to relaxation of residual stresses. A possible additional factor is a homogenization of the dislocation structure as a result of the treatment-induced movement of dislocations.

The present investigation is concerned with the effect of PMF treatment on the corrosion behaviour of titanium in a 0.9% NaF solution. The work showed that the number of dislocations in the treated sample had increased and they exhibited an ordered pattern creating a homogenous sub-microstructure of metal. For the first time, evidence of Frank–Read sources activated by PMF treatment in titanium was observed. The results of corrosion testing show an increase in the corrosion resistance and it can be concluded that the dominant mechanism leading to this behaviour is electrochemical homogenization of surface resulting in a decrease of the potential difference between anodic and cathodic zones and in the formation of denser and finer corrosion products with higher adhesion to the base material.

Methodology

Titanium commercially pure grade 2 (CA TA2) was used during the research. The chemical composition of the material is shown in Table 1. Rectangular samples with dimensions 11 mm x 14 mm were cut from CP TA2 sheet of 0.75 mm thickness using a Struers Secotom-10 cutoff machine with a silicon carbide wheel under minimal feed and intensive liquid cooling. Samples were conditioned by grinding with running water and then polished. Samples in the initial (untreated) and PMF-treated conditions were used for the immersion corrosion and potentiodynamic polarization tests. Characterization of the metals was carried out using light microscopy, transition electron microscopy (TEM), scanning electron microscopy (SEM) and atomic force microscopy (AFM). Microhardness tests were also conducted for samples in the initial and PMF treated states.

A schematic diagram of the generator that was used for the PMF treatment is shown in Fig. 1a. The treatment was fulfilled by the discharge of capacitors of capacitance C = 100 μF that had been charged up to a voltage U = 5 kV. The electric current flowing into the circuit during discharging was registered using a calibrated Rogovsky belt (coil). A typical example of the registered electric current from the treatment is presented in Fig. 1b.

Each sample was treated once per side at room temperature. During the treatment, a sample was pressed to the inductor (four turns of copper bus) as shown in Fig. 2 placing the polished plane to the inductor. The generated electric current passed through the inductor turns producing the magnetic field. The magnetic field induced eddy currents into the sample and these eddy currents in turn produced their own magnetic field. Therefore, during the treatment a sample was exposed simultaneously to PMF and PEC (eddy currents).

The effect of PMF treatment on the corrosion resistance of the samples was investigated by performing static immersion tests in 0.9 % sodium fluoride (NaF) solution. The solution was prepared by dissolving NaF (Fisher Chemicals) in deionized water. The pH was then set to a value of 6.0 using citric acid ($C_6H_8O_7$) (Fisher Chemicals). The pH measurements were carried out using a WTW Series INOLAB Ph 720 pH meter. Three samples were used for each investigated

condition (reference samples without PMF treatment and samples after PMF). Prior to the immersion experiments, the samples were cleaned in acetone using an ultrasonic bath and dried in hot air. Each sample was loaded into an individual volumetric plastic container with the solution. The containers with the loaded samples were placed into a circulating water bath at a controlled temperature of 37˚C (±1˚C) for 120 hours. The NaF solution that was used was prepared in one single batch to ensure uniform conditions throughout the tests. The solution was stirred for 24 hours before use in the immersion tests. The concentration of the Ti ions released to the solution after the corrosion immersion tests was analyzed by means of induced coupled plasma optical emission spectrometry (ICP) (Varian 710-ES). The ICP method was used to evaluate the level of corrosion of the TA2 samples. The morphology of the samples following the immersion tests was examined by means of scanning electron microscopy (SEM) using a JEOL JCM-5700 CarryScope equipped with energy dispersive X-ray microanalysis attachment (EDAX).

In order to identify metallographic differences in samples without and with PMF treatment light microscopy was used. The cross-sections of specimens were cut off and chemically etched using Kroll's reagent. Following etching, the samples were examined using a light microscope (LEITZ Metallux II) equipped with a digital camera. In addition, transmission electron microscopy (TEM) (Tecnai G2 20 Twin) was used. Microhardness tests were fulfilled using a tester (Struers DuraScan-20) under a 2 N load. Measurements were conducted in two ways: (i) along the length of a flat (treated) surface of the specimen, with a distance of 100 μm between indentations and (ii) along the cross-section of the specimen (perpendicularly to two edges), with a distance of 50 μm between indentations and 50 μm from the edge.

Atomic force microscope (AFM) (Nanosurf Easyscan 2) was used to identify changes in the surface topography of samples after the treatment. The same sample was used to characterize the surface before and after treatment. The scanned area had dimensions of 60 μm x 60 μm. Taking into account the fact that this examination must be conducted at the same site of the specimen surface, the specific pattern of imprints (imprint pattern of orthogonal array of 4x4 imprints with a

distance of 20 μm between imprints) was applied before the tests to help identify the position of the cantilever tip under the site of the measurements. These imprints were made using a Struers DuraScan-20 tester under a minimal load. The scan head of the microscope was equipped by a cantilever with a conductive Cr/Pt-coated tip and an AC voltage of ±2 V of high frequency which was applied to the tip to obtain not only surface topography data, but also data of the current passing through the tip.

Results

ICP results showing the level of dissolution of titanium ions after immersion tests are presented in Table 2. A quantitative comparison of the amount of released Ti ions from untreated and PMF treated samples is demonstrated in Fig. 3. Based on the obtained ICP results it can be concluded that the release of titanium ions after exposure in sodium fluoride solution in the PMF treated sample was reduced by 16% in comparison with the untreated one.

Morphological and compositional data of the untreated and treated samples following the immersion test are presented in Figs. 4, 5 and 6 and in Table 4. In Fig. 4a and 5a, micrographs of the microstructure of untreated and treated samples are presented. Even though the microstructure for the untreated and treated samples (Fig. 4a and 5a) show an almost complete coincidence and lack of any significant differences, the SEM micrographs demonstrate a substantial difference between the morphology of the corrosion products of the untreated and PMF treated samples. The corrosion products for the treated sample are finer in comparison with the rough corrosion products on the untreated sample. Figs. 4b and 4c also show that a visible network of continuous lines of the corrosion product (lighter lines) exists and it has a cellular pattern and in a considerable degree reproduces the grain microstructure of the material revealed by chemical etching (see Fig. 4a). Some parts of the corrosion product seem to protrude above the other areas. EDAX elemental microanalysis scanning results along the white indicated line on the surface of untreated sample (Fig. 6) show substantially higher levels of fluorine and sodium in these lighter

areas and from this it was concluded that these areas were thicker. In these areas the corrosion product is probably formed just above the grain boundaries due to more corrosion at these areas.

In contrast, in the case of the treated sample, the corrosion products are uniformly distributed on the metal surface and show evidence of orientation. At the same time, according to X-ray diffraction and EDAX analysis (Fig. 7, Table 3) it can be concluded that the surface of the tested samples in both conditions (with and without PMF treatment) after immersion tests is covered by a corrosion product of sodium hexafluorotitanate Na_3TiF_6. In addition, areas of cracking and delamination of the corrosion product on the surface of the untreated sample were observed (Fig. 8a), while no cracks were observed on the surface of treated sample (Fig. 8b).

The TEM examination shows a significant change in the dislocation network following PMF treatment. There seems to be a lower density of dislocations in the untreated sample (Fig. 9a), while at the same time they are tangled up. Following PMF treatment, the dislocation density seems to have increased as shown in Fig. 9b and they are no longer tangled up, but they are uniformly dispersed within the metal. In addition, the dislocations show some orientation.

The results of microhardness measurements are presented in Table 4 and it is shown that there was a slight increase in the microhardness of samples as a result of PMF treatment. At the same time it can be observed that the standard deviation in the microhardness values was lower for the PMF treated samples indicating that for these samples there was a lower scatter in microhardness measurements.

Atomic force microscopy scanning results for the same sample before and after PMF treatment are presented in Fig. 10 which shows evidence of changes in the surface topography of the specimens after the PMF treatment. The change in the topography profiles suggest that the PMF treatment led to residual microplastic deformation. Using the Nanosurf Easyscan 2 control software the average value for the electric current, I_a, flowing through the tip of the measuring cantilever were calculated according to the formula:

$$I_a = \frac{1}{MN} \sum_{k=1}^{M} \sum_{l=1}^{N} | i(x_k, y_l) |,$$

where $i(x_k, y_l)$ are electric current data at points within the selected area.

Data for the currents (Table 5) can be used to estimate the spread of the electrical resistivity of the surface material. It can be observed that for the entire scanned surface areas shown in Figs. 10a and Fig.10b, the electrical resistivity after the treatment increased by 14%, while for the line AB the increase was 17%.

Discussion

The effect of PEC and PMF treatment on the mechanical properties (hardness, fatigue strength, wear resistance) of structural metals is well known, but the reasons and the driving mechanisms of their effect (with the exception of heating) are not well-defined to date. This kind of treatment is relatively new for corrosion mitigation and apart from the work of the present authors[12, 13] and a small number of other researchers[14, 15] very little has been reported. Fang et al[14] demonstrated that direct passage of a PEC improved the resistance to stress-corrosion cracking of pipeline steels. This effect was attributed to grain refinement which resulted from ferrite↔austenite solid-state phase transformation. It was reported that the treatment of current density of 8.3 kA/mm^2 had led to heating of the steels into the austenitic region. Heating as a result of PEC treatment also led to improvement of nickel-based alloys against intergranular corrosion[15].

However, in the present research, the samples showed no evidence of substantial heating during the application of the PMF as the experimentally measured temperature values were 37 - 40 °C. The applied treatment was affected by both PMF and PEC in the form of eddy currents. Finite element analysis using QuickField 6 software was employed to determine eddy currents and field

distributions as well as the heating effect of the PEC and PMF treatments. This was conducted in two steps; the first step involved the solution of a sub-problem of the transient electromagnetic field, while the second was based on a solution of a sub-problem of transient heating caused by Joule loss (the capacity of heat generation from the first step was used). The sub-problems were solved in 2-D formulations. The calculations were carried out using the following physical properties of titanium: density ρ = 4.5 Mg.m^{-3}, coefficient of thermal expansion α = 1.25·10^{-5} K^{-1}, electrical conductivity σ = 1.794·10^{6} S.m^{-1}, thermal conductivity λ = 22 W/(m·K) and specific heat c = 523 J/(kg·K). All the properties in the calculations were assumed to be independent of temperature. The relative permeability was taken as μ = 1 due to the high magnetic field strength that was produced under the treatment. Heat exchange with air was not taken into account due to the short duration of the treatment and zero initial conditions were assigned. The variation of a full current passing through the inductor was in the form of a decaying sinusoid $I(t) = I_0 \exp(-a \cdot t / t_{PEC}) \sin(2\pi t / t_{PEC})$, where t_{PEC} is a period of current oscillation. The values of I_0, a and t_{PEC} were determined using the registered profiles of the PEC based on best fitting. Calculations were carried out for a time equal to 300 μs (see Fig. 1b).

The results of the numerical modeling of the treatment are presented in Figs. 11 and 12 which show that the magnetic field strength was H = 1.2 – 1.3 MA/m and the induced eddy currents had a current density j = 1.1 – 1.4 kA/mm^2. The temperature increase was calculated to be 17 K. This result was in agreement with the experimentally measured values. From this analysis, it is clear that the observed increase in the corrosion resistance was unlikely to be due to heating effects. A more likely cause of this observation may be due to changes in the residual stresses in titanium as a result of PMF treatment which has previously been reported to cause stress relaxation in metals. This effect can be explained by the increasing mobility of dislocations due to application of PEC or PMF treatments. Stress relaxation has been reported[16] to occur when the electric current density exceeds a threshold value which has been estimated to be about 1 kA/mm^2. According to the

simulation results in Fig. 11a, the eddy current densities on the surface of PMF treated samples was in excess of 1 kA/mm^2.

The present research has shown a decrease in the scattering of the microhardness values for the PMF treated samples in comparison with the untreated ones. Measurement of the indentation hardness has been reported to represent the residual stress state of metals[17]; a lower hardness within the same material may represent the presece of tensile residual stresses, while higher hardness may reflect compressive ones. Hence, lowering of the hardness scatter can be a result of microstructural homohenization within a material including reduction of residual stresses.

The mechanism for this lies in the dislocations multiplication and reordering caused by the PMF treatment. The TEM observations have shown a significant change in the dislocation network in the untreated (Fig. 9a) and PMF treated (Fig. 9b) samples. The number of dislocations in the treated sample has increased and they all have an ordered pattern. A uniform pattern of dislocations in steel as a result of PMF treatment has previously been observed by Wu et al[18], but the ordering of the dislocation network as presented in Fig. 9b has not been reported before. Ma et al[19] also observed an increase in the number of dislocations in steel as a result of magnetic treatment and proposed this to be due to a "magneto-stress" acting on the dislocations when the ferromagnetic steel was exposed to it. As a result, Frank–Read sources became activated and dislocation slip increased the dislocation density. The force responsible for the "magneto-stress" was based on the value of the magnetization of steel. However, titanium is paramagnetic and its magnetization is several orders of magnitude lower than steel and therefore this approach cannot be used to explain the observations in the present research.

The effect of the pulsed eddy currents on the metallic crystal lattice of titanium can be analyzed by using the basic relationships that determine the kinetics of the interaction between the conductivity electrons and the crystal lattice in accordance with existing notions of the electronic conductivity mechanism[20]. These allow the estimation of the current density, the electric field intensity and the electrical resistivity as presented in the equations below:

$$
\begin{aligned}
& i = e\, v\, n_0; \\
& \frac{dU}{dx} = E = \rho\, i; \\
& \rho = \frac{2m_e}{n_0 e^2 t_0},
\end{aligned}
\tag{1}
$$

where i is the current density in A/m^2, e is the electron elementary charge, v is the velocity of the electron drift in m/s, n_0 is the number of conductivity electrons per unit volume (1/m^3), U is the electric potential in V, E is the electric field intensity in V/m, ρ is the electrical resistivity in Ω·m, m_e is the electron rest mass which is equal to $9.10956 \cdot 10^{-31}$ kg, l_0 is the mean free path of electrons in m and t_0 is the mean free time of electrons between ionic collisions. From these equations, the kinetic energy, K_e, of the electron drift (electron wind) by the action of the electric field under isotropic scattering of electrons can be derived as

$$
K_e = m_e v^2 / 2 = e E \cdot (v t_0) = \rho i (e v n_0) \frac{t_0}{n_0} = \rho i^2 \frac{t_0}{n_0}
\tag{2}
$$

The parameters for interaction between electrons and the crystal lattice can be estimated by using the equations above. The increase in the kinetic energy of an electron within its free path calculated by equation (2) at a current density of 10 kA/mm^2 yields $\Delta K_{e(Ti)} \cong 9.6 \times 10^{-12}$ eV/atom for titanium. These values are much lower than the change in the thermal motion energy, ΔK_T, of titanium atoms at an increase in temperature by 1°C (which equals $\Delta K_T \cong kT \cong 8.61 \times 10^{-5}$ eV/atom). Thus, a single interaction between an electron and an atom does not exert significant influence on the motion of a metallic atom in a perfect crystal lattice.

However, when assessing the effect of a pulsed electric current (eddy current) on the dislocation dynamics, the preferential interaction between flow electrons and atoms in the vicinity of dislocations and other defects must also be considered. In this case if the ratio of the total density of atoms, n, to the density of "defective" atoms, n_d, (atoms in the vicinity of defects like grain boundaries, dislocations, vacancies, etc.), n/n_d is about $2 \cdot 10^6$ and this corresponds to a dislocation density of about 10^9/m^2 and the mean effective increase of the kinetic energy of all the

"defective" atoms in titanium can be evaluated as $\Delta K_{ef(Ti)} \cong 1.9 \cdot 10^{-5}$ eV/atom. Evaluating the increase of the kinetic energy of atoms by using equation (2), the mean free time between ionic collisions, t_0, was used. In the presence of defects, the relaxation time for defect scattering, t_r, needs to be taken into account and this value is greater than t_0 because in this case scattering requires more scattering events and the relaxation time is longer than for isotropic scattering. By using equations (1), the value of t_0 for titanium can be calculated to be 9.5 x 10^{-16} s, while the relaxation time for electron-phonon scattering in metals is of the order of a few picoseconds. Assuming, for example, for titanium atoms a value of t_r of about 2 x 10^{-12} s, the interaction of the conductivity electrons with "defective" atoms during the time of relaxation enhances the energy of the ordered "defective" atom motion (motion of dislocation) under the action of the electron flow by $\Delta Q_e = (t_r / t_0) \cdot K_{ef}$ or 1.4 x 10^{-2} eV/atom. This corresponds to equivalent heating up to temperature $T_{eq} = \Delta Q_e / k \approx 160$ K.

Data for ΔQ_e and T_{eq} calculated using the above approach are presented in Fig. 13 which demonstrates that within reasonable current densities (up to 10 kA/mm^2) the level of kinetic energy of the ordered motion of dislocation is not very high and the corresponding equivalent heating is not enough to support rearrangement of the microstructure. Some microstructural changes can be expected during treatment at around 20 kA/mm^2, but the generation of eddy currents with a current density of this level is not easy. At the same time the current acts within some period of processing time and this also should be taken into account. For example, results of open-boundary non-adiabatic molecular dynamics simulation of the atom which is driven by the non-conservative current-induced force[21] show an exponential increase in the kinetic energy during time of electric current action.

Therefore electron wind can potentially cause movement of dislocations which may become pinned by impurity atoms (in this case iron which is available as an impurity in the material) and the Frank–Read sources can be activated and hence dislocation multiplication may take place. Evidence of Frank–Read sources can be observed in the TEM results presented in Fig. 9c. The

white arrows show dislocations which have been pinned acting like Frank–Read sources. The increase in the number of dislocations was accompanied with an increase in the microhardness of the PMF treated samples as reported in Table 5. As a consequence, an increase in the surface electrical resistivity (Table 5) was observed as the increasing number of dislocations acted as obstacles to the current flow during measurements.

Generally an increase in the concentration of dislocations at specific areas within a metal (for example, at grain boundaries) results in a reduction in the corrosion resistance because these areas become anodic and this makes the material locally more active[22, 23]. The TEM investigation has shown evidence of localized pinning of dislocations resulting in areas of high concentration of dislocations within the untreated samples; this localized concentration is the reason for the higher corrosion rate for samples in the untreated condition as the areas of localized dislocations exhibit a high anodic character. The samples that had undergone PMF treatment showed higher corrosion resistance in spite of the fact that they contained a higher number of dislocations. This was due to the fact that the dislocations in the samples following PMF treatment were not tangled up locally, but they were dispersed within the structure and appeared to provide more homogeneous behaviour within the structure. This homogenization promotes micro-electrochemical homogenization of the surface of the treated metal causing a decrease of the current densities of all anodic and cathodic reactions across the surface of metal. As a consequence, the formation of the corrosion products takes more slowly and there exist more nucleation sites leading to a denser and finer corrosion product (Fig. 5c) with better adhesion to the material surface. The corrosion products serve as a protective coating and enhance the resistance to the corrosion.

Other recent research has demonstrated similar effects; for example, different processing techniques which are accompanied by substantial generation of dislocations like friction stir processing[24], high-current electron beam processing[25], pulsed electron beam processing[26, 27], equal channel angular pressing[28] as well as treatments like surface mechanical attrition processing show that they cause microstructural homogenization resulting in improved corrosion resistance.

The effect on corrosion of the homogenization of the dislocation structure and reduction of residual stresses as observed in the current work can be explained by using the diagram in Fig. 14. This model contains four grains of a material along some direction *x*. The initial state of the metal (Fig. 14a) is characterized by a low number of dislocations which are pinned near grain boundaries, while the metal following PMF treatment (Fig. 14b) is characterized by a higher number of dislocations that are dispersed within the structure. It is considered that the residual stresses in the metal can have different values and signs (positive or negative) from grain to grain depending on the primary crystallographic orientation of the rolling direction, etc. So, it is proposed that the distribution of residual stresses along the *x* direction in the case of initial material corresponds to Fig. 14c, and the distribution of a reduced level of residual stresses after PMF treatment along the same direction corresponds to Fig. 14d.

In the untreated state of metal (Fig. 14e) the tensile residual stresses in grains 1 and 3 determine the anodic (negative) potential of the grains and compressive residual stresses in grains 2 and 4 determine the cathodic (positive) potential of the grains. Clusters of dislocations near the grain boundaries locally increase the anodic potential. This can be a reason for the observed preferable corrosion along grain boundaries of untreated samples presented in Figs. 4b, Fig.4c and Fig.6.

PMF treatment (i) creates a network of ordered dislocations of high density (Fig. 14b) and (ii) decreases and redistributes residual stresses within grains (Fig. 14d). This network of dislocations can increase the general anodic potential at the surface of the treated metal (Fig. 14f), but due to a treatment-induced reduction of residual stresses, a variation of the potential along the surface can be much lower than in the case of the metal in the initial state. As shown in Fig. 14e and Fig. 14f for the initial state, a difference in the potentials between grains 1 and 2 ($\Delta\varphi_{12}^{\text{init}}$), between grains 2 and 3 ($\Delta\varphi_{23}^{\text{init}}$) and between grains 3 and 4 ($\Delta\varphi_{34}^{\text{init}}$) is much lower than the differences $\Delta\varphi_{12}^{\text{treat}}$, $\Delta\varphi_{23}^{\text{treat}}$ and $\Delta\varphi_{34}^{\text{treat}}$ in the treated one. Lower differences in potential will cause lower galvanic currents. Therefore due to such micro-electrochemical homogenization of the surface of the

treated metal, the current densities of all anodic and cathodic reactions will be substantially reduced. This causes a suppression of the micro-galvanic couple effect in the material, more slow formation of the corrosion products in more nucleation sites leading to a denser and finer their structure with better adhesion to the substrate thus enhancing its corrosion resistance.

Conclusions

Based on the results of the investigation, the following conclusions were drawn:

1. Processing commercially pure titanium by pulsed magnetic field leads to significant change in the dislocation network leading to an increase in the dislocation density. At the same time the dislocations that were tangled up at grain boundaries prior to pulsed magnetic field treatment became untangled and the dislocations were observed to be uniformly dispersed within the metal and to exhibit specific orientation which can coincide with direction of the eddy currents induced during treatment.

2. The generation of dislocations and their ordering can be explained by the interaction between the conductivity electrons and atoms of the crystal lattice: treatment-induced electron wind (eddy currents) causes movement of dislocations pinned by impurity atoms and Frank–Read sources are activated and dislocations multiplication as well as ordering take place. This leads to surface microplastic deformation, reduction of microhardness scattering, increase of the electrical resistivity of treated metal and possibly to reduction of residual stresses.

3. Pulsed magnetic field treatment leads to micro-electrochemical homogenization of the surface of titanium causing a decrease in the current densities of all anodic and cathodic reactions across the surface of metal during corrosion tests and as a result to formation of denser and finer corrosion products with higher adhesion to the substrate. This promotes an increase of the corrosion resistance of treated metal.

Acknowledgement

This research was supported by the Marie Curie International Incoming Fellowship scheme within the 7th European Community Framework Programme Grant number PIIF-GA-2010-274324 and COST Action: MP1005 (ECOST-STSM-MP1005-010512-016210).

1. F. Di Carlo, C. Cassinelli, M. Morra, L.F. Ronconi, M.A. Bassi, G. De Muro, A. Quaranta: "Corrosion of titanium in presence of dental amalgams and fluorides". *Minerva Stomatologica*, 2003, **52**, 111-121.
2. N. Schiff, M. Boinet, L. Morgon, M. Lissac, F. Dalard, B. Grosgogeat: "Galvanic corrosion between orthodontic wires and brackets in fluoride mouthwashes", *European Journal of Orthodontics*, 2006, **28**, 298-304.
3. K. Kaneko, K. Yokoyama, K. Moriyama, K. Asaoka, J. Sakai, M. Nagumo: "Delayed fracture of beta titanium orthodontic wire in fluoride aqueous solutions", *Biomaterials*, 2003, **24**, 2113-2120.
4. M. Nakagawa, S. Matsuya, K. Udoh: "Corrosion behavior of pure titanium and titanium alloys in fluoride-containing solutions", *Dental Materials Journal*, 2001, **20,** 305-314.
5. J. J. Harwood: "The influence of stress on corrosion (Part 1 of Two Parts)", *Corrosion*, 1950, **6,** 249-259.
6. O. Takakuwa, H. Soyama: "Effect of residual stress on the corrosion behavior of austenitic stainless steel", *Advances in chemical engineering and science*, 2015, 5, 62-71.
7. B. E. Klamecki: "Residual stress reduction by pulsed magnetic treatment", *Journal of Materials Processing Technology*, 2003, 141, 385–394.
8. F. Tang, A. L. Lu, J. F. Mei, H. Z. Fang and X. J. Luo: "Research on residual stress reduction by a low frequency alternating magnetic field", *Journal of Materials Processing Technology*, 1998, 74, 255–258.

9. Z. P. Cai, J. A. Lin, L. A. Zhou and H. Y. Zhao: “Evaluation of effect of magnetostriction on residual stress relief by pulsed magnetic treatment”, *Materials Science and Technology*, 2004, 20, 1563–1566.
10. S. Wu, H. Y. Zhao, A. L. Lu and H. Z. Fang: “Micro mechanism of reducing residual stress by low frequency alternating magnetic treatment”, *Transactions of the China Welding Institution*, 2002, 23, 10–11.
11. G. Stepanov, A. Babutskii, I. Mameyev, M. Ferraris, V. Casalegno and M. Salvo: “Experimental evaluation of pulse electric current effect on residual stresses in composite-to-copper joints”, Strength of Materials, 2008, 40, 452-457.
12. A. Babutsky, A. Chrysanthou and J. Ioannou: “Influence of pulsed electric current treatment on corrosion of structural metals”, Strength of Materials, 2009, 41, 487-491.
13. L. Kruszka, A. Babutsky, A. Chrysanthou and C. E. Tan: “Effect of pulsed electric current treatment on the corrosion and strength of reinforcing steel”, *Materials Science Forum*, 2012, **706-709**, 937-944.
14. B. Fang, J. Wang, S. Xiao, E.-H. Han, Z. Zhu and W. Ke: “Stress corrosion cracking of X-70 pipeline steels by eletropulsing treatment in near-neutral pH solution”, *Journal of Material Science*, 2005, **40**, 6545–6552.
15. Y. Liu, L. Wang, H. Liu, B. Zhang and G. Zhao: “Effect of electropulsing treatment on corrosion behavior of nickel base corrosion-resistant alloy”, *Transactions of Nonferrous Metal Society of China*, 2011, **21**, 1970-1975.
16. Y.V. Baranov, O.V. Troitskii, Y.S. Avraamov and A.D. Shlyapin: “Physical bases of electric-pulse and electroplastic treatments and new materials”, Chap. 1, “Electroplastical deformation of metals”, 56-77, 2001, Moscow, MGIU.
17. J. Jang: “Estimation of residual stress by instrumented indentation: A review”, *Journal of Ceramic Processing Research*, 2009, **10**, 391-400.

18. S. Wu, H. Zhao, Lu Anli, H. Fang and F. Tang: “A micro-mechanism model of residual stress reduction by low frequency alternating magnetic field treatment”, *Journal of Materials Processing Technology*, 2003, **132**, 198-202.
19. L. Ma, W. Zhao, Z. Liang, X. Wang, L. Xie, L. Jiao and T. Zhou: “An investigation on the mechanical property changing mechanism of high speed steel by pulsed magnetic treatment”, *Materials Science and Engineering*, 2014, **A609**, 16–25.
20. R.W. Christy and A. Pytte: “The Structure of Matter: An Introduction to Modern Physics” 1965, New York, Amsterdam, W.A. Benjamin Inc.
21. D. Dundas, E. J. McEniry and T. N. Todorov: “Current-driven atomic waterwheels”, *Nature Nanotechnology*, 2009, **4**, 99–102.
22. N. Perez: “Electrochemistry and corrosion science”, Chap. 2 “Electrochemistry”, 27-70, 2004, New York, Boston, Dordrecht, London, Moscow, Kluwer Academic Publishers.
23. E. Bardal: “Corrosion and protection”, Chap. 7, “Different forms of corrosion classified on the basis of appearance”, 89-192, 2004, London, Berlin, Heidelberg, Springer-Verlag.
24. A.G. Rao, V.A. Katkar, G. Gunasekaran, V.P. Deshmukh, N. Prabhu and B.P. Kashyap: “Effect of multipass friction stir processing on corrosion resistance of hypereutectic Al–30Si alloy”, *Corrosion Science*, 2014, **83**, 198–208.
25. Z. Zhang, S. Yang, P. Lv, Y. Li, X. Wang, X. Hou and Q. Guan: “The microstructures and corrosion properties of polycrystalline copper induced by high-current pulsed electron beam”, *Applied Surface Science*, 2014, **294**, 9–14.
26. J. Kim, S. S. Park and H. W. Park: “Corrosion inhibition and surface hardening of KP1 and KP4 mold steels using pulsed electron beam treatment”, *Corrosion Science*, 2014, **89**, 179–188.
27. J. Kim and H. W. Park: “Influence of a large pulsed electron beam (LPEB) on the corrosion resistance of Ti6Al7Nb alloys”, *Corrosion Science*, 2015, **90**, 153–160.

28. H. Miyamoto, K. Harada, T. Mimaki, A. Vinogradov and S. Hashimoto: “Corrosion of ultra-fine grained copper fabricated by equal-channel angular pressing”, *Corrosion Science*, 2008, **50,** 1215–1220.

Table 1

Nominal chemical composition of CP TA2 (grade 2), weight %

Ti	C	Fe	N	O	H
Balance	0.10	0.30	0.03	0.25	0.015

Table 2

ICP results of dissolved Ti ions after immersion of the samples without and with PMF treatment

Specimens	Concentration of released Ti ions, mg/l	
	Mean	SD
Untreated	159.12	1.42
PMF treated	134.40	0.82

Specimens were loaded into containers with the solution on the basis of 1 ml solution for 16 mm^2 of a specimen's area. SD – standard deviation.

Table 3

EDAX elemental spot analysis of the corrosion product on samples surface

Element	Untreated (Fig. 7a, 7b)		Treated (Fig. 7c, 7d)	
	Wt%	At%	Wt%	At%
SiK	0.83	0.73	0.86	0.74
FK	39.77	51.83	39.71	50.89
NaK	29.88	32.18	32.99	34.93
TiK	29.52	15.26	26.45	13.44

Table 4

Microhardness of untreated and PMF treated samples

Specimens/conditions	Number of measurements	Microhardness, H_V				
		mean	min	max	SD	SD/mean
Flat face surface of samples						
untreated	56	199	177	227	10.5	0.053
PMF treated	65	205	189	230	8.8	0.043
Cross-section of samples						
untreated	14	197	180	208	9.0	0.046
PMF treated	14	205	195	215	7.3	0.036

Table 5

Currents flowing through a tip of the measuring cantilever

Untreated	I_a, nA	PMF treated	I_a, nA
Complete area on Fig. 11a	89.6	Complete area on Fig. 11b	77.4
Along line AB	92.2	Along line AB	69.6

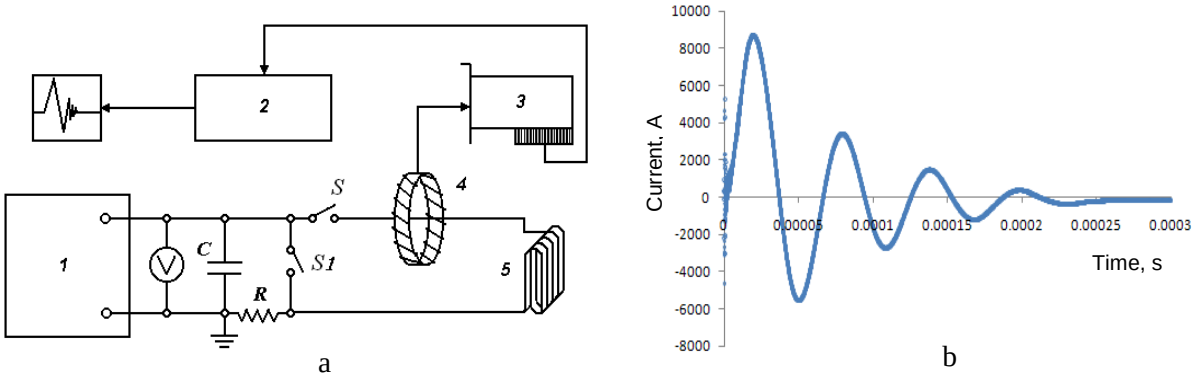

a b

Fig.1

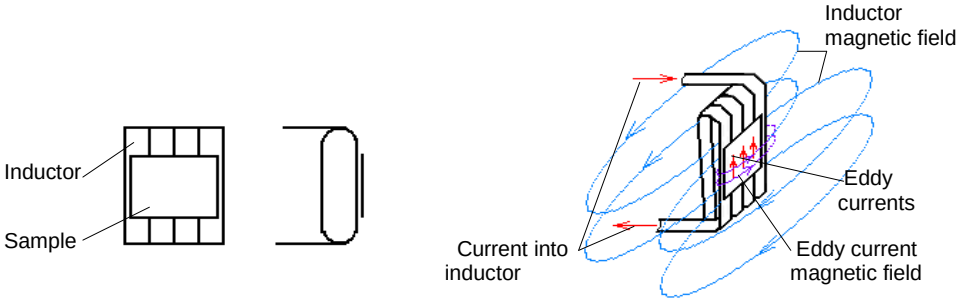

a b c

Fig.2

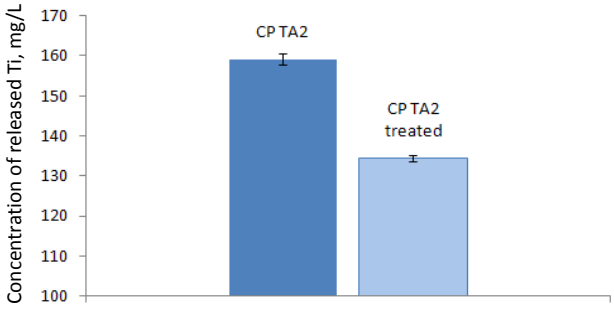

Fig.3.

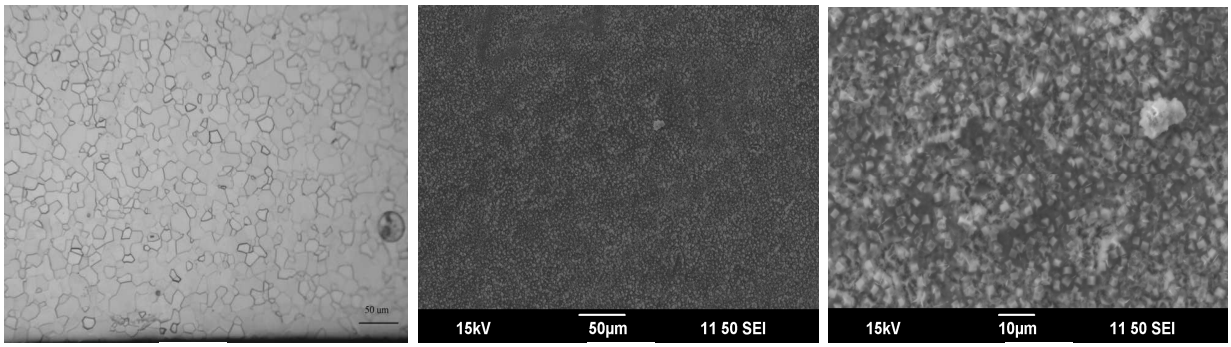

a b c

Fig.4

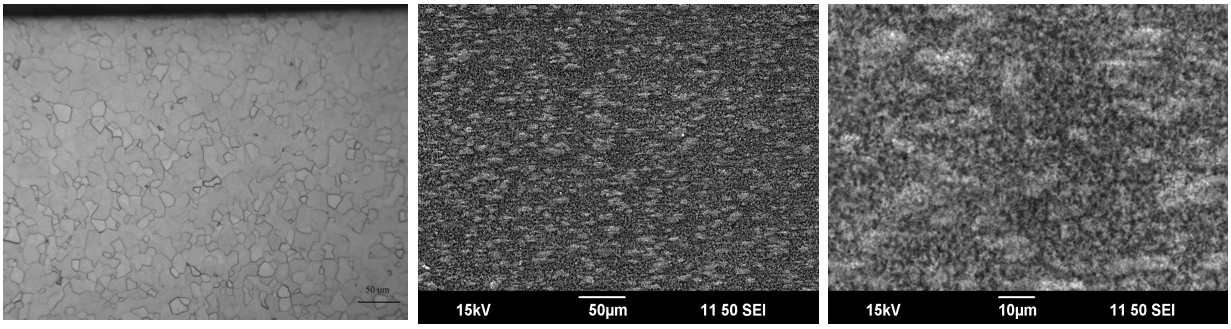

a b c

Fig.5

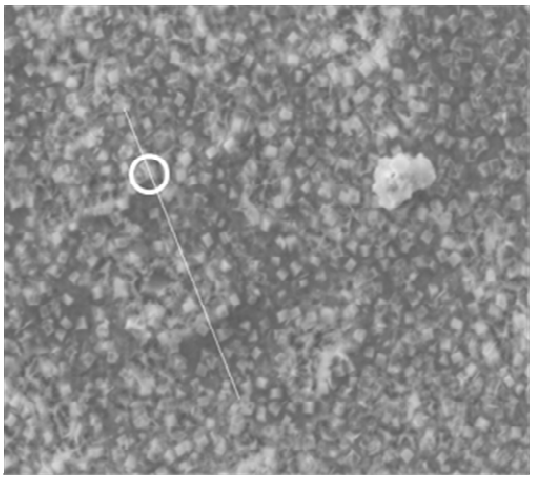

a

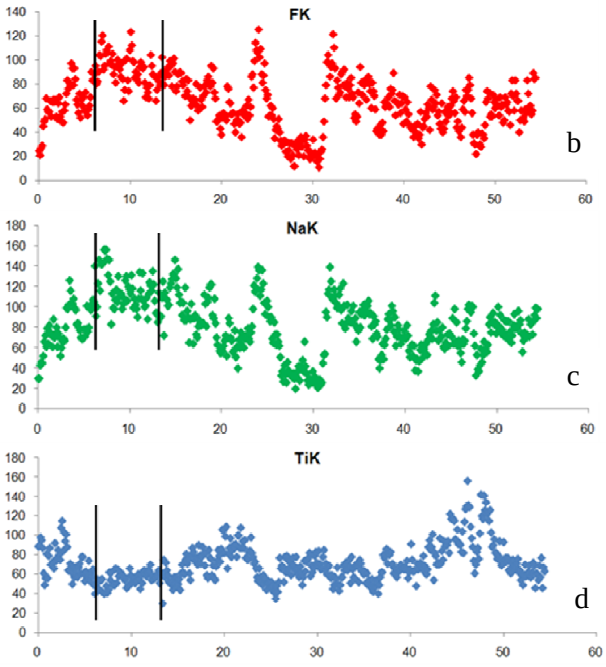

Fig. 6

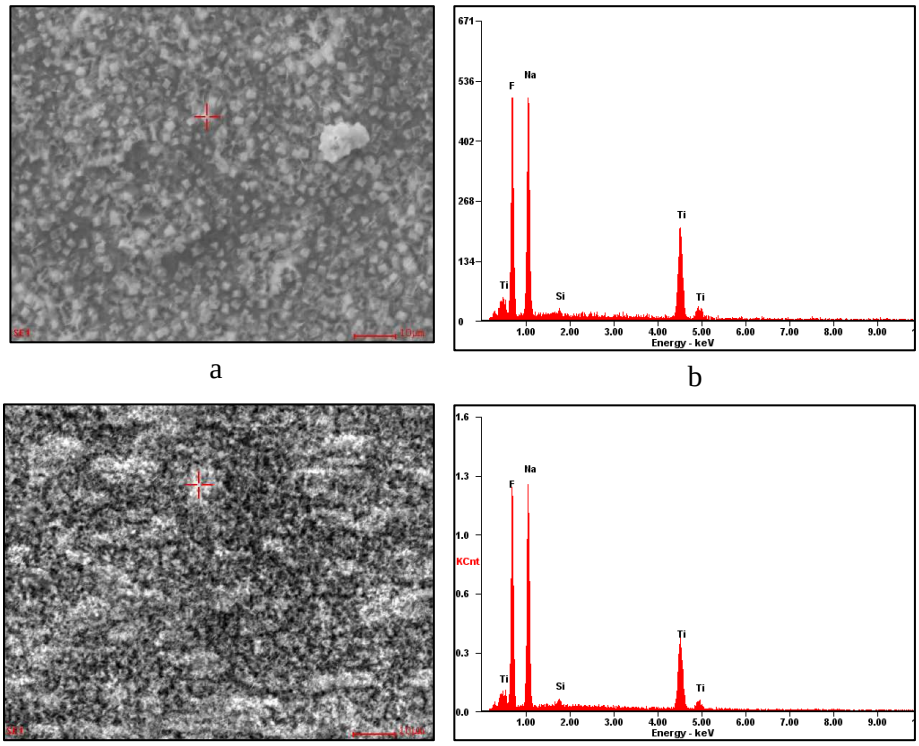

a b

c d

Fig.7

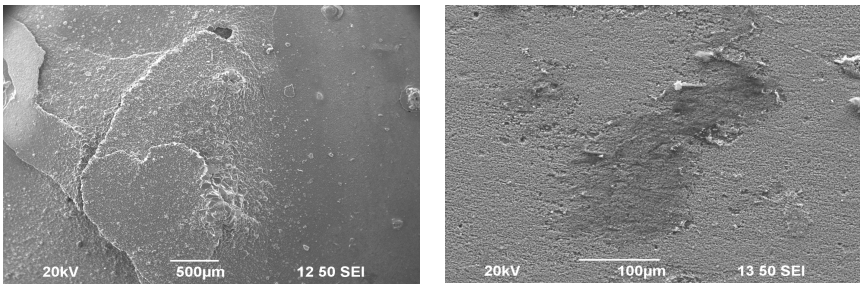

a b

Fig. 8

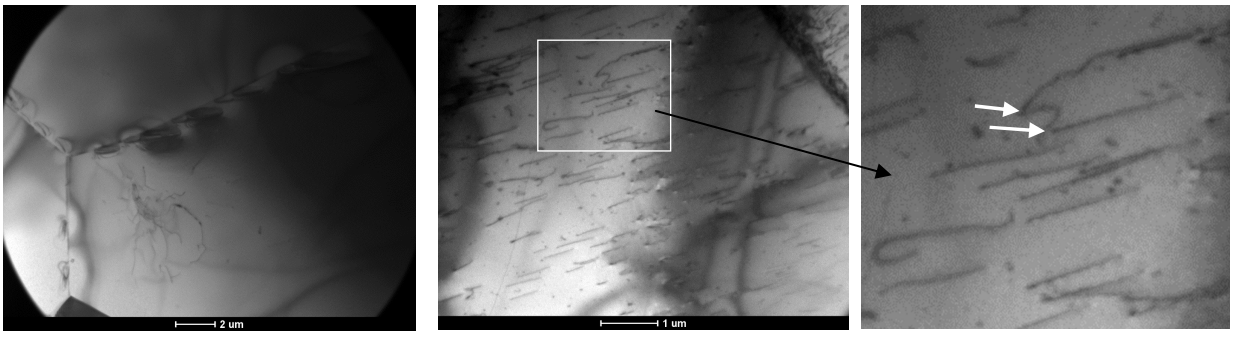

a b c

Fig. 9.

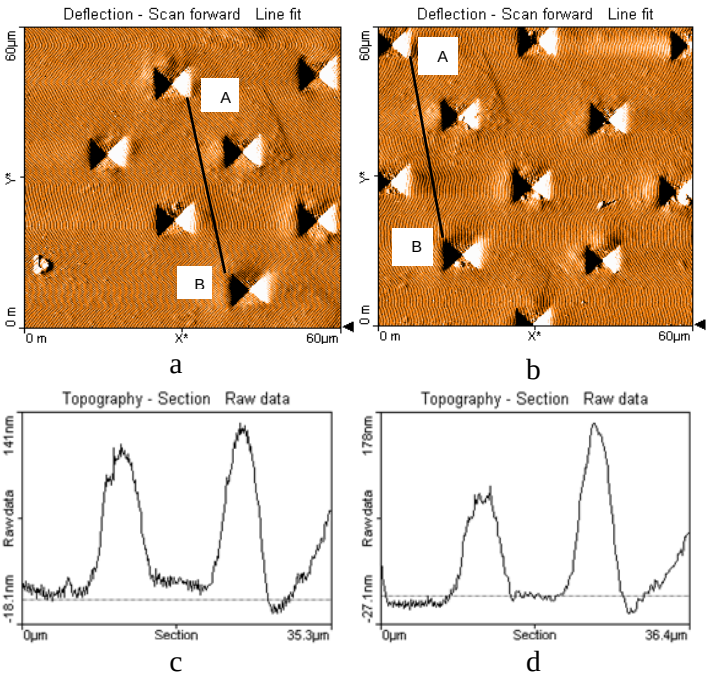

Fig.10.

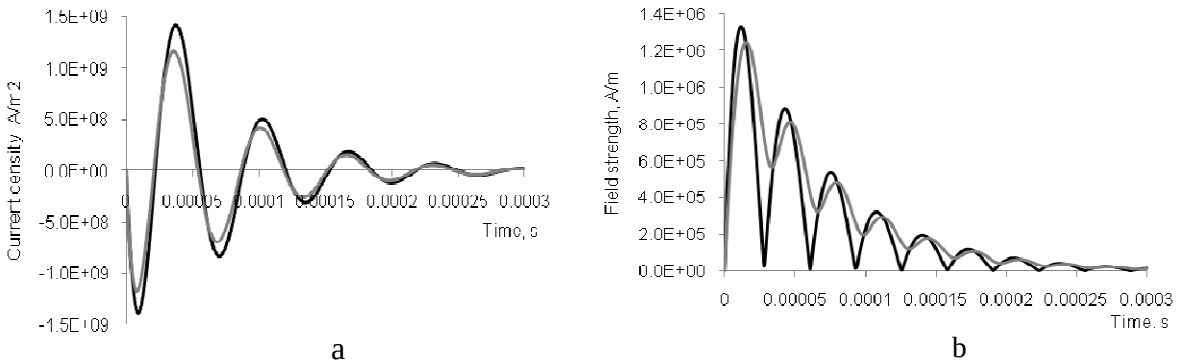

Fig.11.

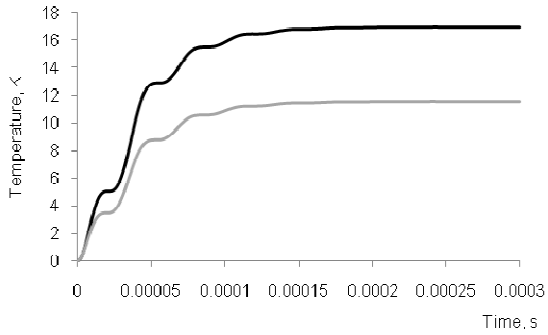

Fig.12

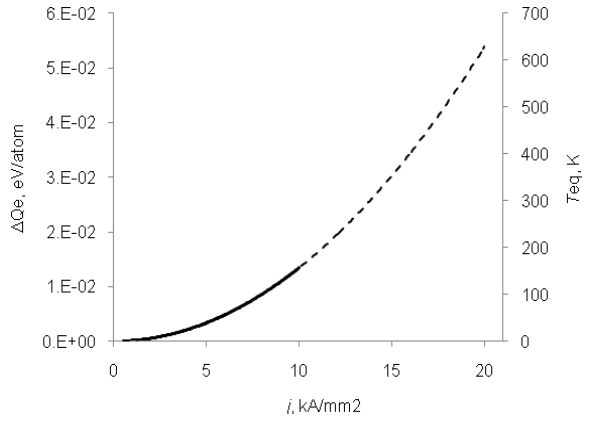
6.E-02
5.E-02
4.E-02
3.E-02
2.E-02
1.E-02
0.E+00
ΔQe, eV/atom
700
600
500
400
300
200
100
0
Teq, K
0
5
10
15
20
i, kA/mm2

Fig.13.

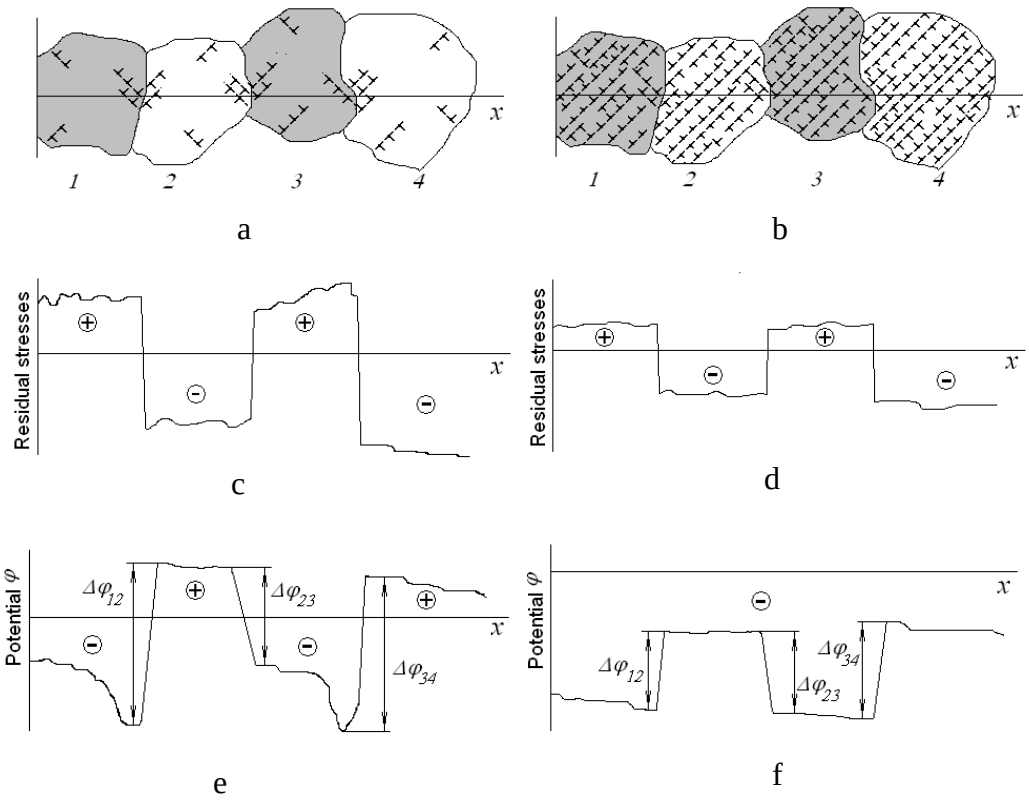
x
1
2
3
4
a
b
Residual stresses
c
d
Potential φ
Δφ12
Δφ23
Δφ34
e
f

Fig.14.

Fig. 1. (a) PEC generator with registration system and (b) a typical example of the registered electopulse in the generator circuit during discharging (U = 5 kV, C = 100 μF): C – capacitor battery, R – ballast resistor, S and S1 – switches; 1 – high voltage supplier, 2 – software, 3 – A-D high frequency converter, 4 – Rogovsky belt (coil), 5 – inductor.

Fig. 2. Sample positioning (a, b – front and side views of inductor with sample) and factors affecting sample (c) during PMF treatment.

Fig. 3**.** Quantitative comparison of released Ti ions from untreated and PMF treated samples after immersion in 0.9 % NaF at pH 6.0.

Fig. 4. Surface of untreated sample after etching (a: light microscopy) and immersion tests (b, c: SEM).

Fig. 5. Surface of treated sample after etching (a: light microscopy) and immersion tests (b, c: SEM).

Fig. 6. EDAX elemental microanalysis scanning results along the white indicated line (from above) on surface of untreated sample (a): b - fluorine (F), c - sodium (Na), d - titanium (Ti) .

Fig. 7. EDAX elemental spot analysis of the corrosion product on samples surface of untreated (a, b) and treated (c, d) samples.

Fig. 8 Corrosion product on the surface of untreated (a) and treated (b) samples.

Fig.9. TEM micrographs of untreated (a) and treated (b, c) samples

Fig.10. AFM scans of the same sample surface before (a) and after (b) treatment and topography data along line AB before (a) and after (b) treatment.

Fig. 11. Variation of density of eddy currents (a) and magnetic field (b) on the surface faced to the inductor in a middle of the sample (black line) and on sample's edge (grey line).

Fig. 12. Heating of the surface faced to the inductor in a middle of the sample (black line) and on sample's edge (grey line).

Fig. 13. Energy of dislocation motion ΔQ_e and temperature of equivalent heating T_{eq} *vs*. applied current density.

Fig. 14**.** Scheme, explaining mechanism of electrochemical homogenization of metal surface under used PMF treatment: (a. b) – elements of structure, (c, d) – distribution of RS, (e, f) – distribution of electrochemical potentials; (a, c, e) – initial state, (b, d, f) – state after the treatment.